



A revisit of the interannual variation of the South China Sea upper layer circulation in summer: correlation between the eastward jet and northward branch

Tingting Zu^{1,2} · Dongxiao Wang¹ · Qiang Wang^{1,2} · Mingting Li³ · Jun Wei³ · Bingxu Geng^{1,2} · Yunkai He^{1,2} · Ju Chen^{1,2}

Received: 15 May 2019 / Accepted: 1 October 2019 / Published online: 16 October 2019
© Springer-Verlag GmbH Germany, part of Springer Nature 2019

Abstract

The interannual variation of the South China Sea upper layer circulation in summer is revisited based on analysis of current derived from altimetry data, Acoustic Doppler Current Profilers moorings, and numerical simulations. Results show not only the interannual variation of the eastward jet (eastward branch), but also its anti-correlation with the northward branch. On interannual time scale, when the eastward branch is enhanced, the northward branch is weakened, and vice versa. Their variations are largely related to the change of the South China Sea summer monsoon (SCSSM), and are strongly influenced by the Luzon strait Transport (LST). Composite analysis reveals a stronger SCSSM and LST into the SCS in the developing phase of El Niño would lead to an eastward branch dominant circulation pattern, whereas a weaker SCSSM and reduced LST into the SCS in the decaying phase of El Niño favors a northward branch dominant circulation pattern. The distinct composite patterns appear in El Niño and Southern Oscillation cycles, rather than episodic event or multiyear El Niño or La Niña. Contribution of the transport of major straits in the SCS to the interannual variation of the SCS summer circulation is quantitatively evaluated for the first time, and the results show that the change of the planetary vorticity flux through three major straits (Luzon strait contributes most) is as equally important as the vorticity input change from local wind stress curl.

Keywords Interannual variability · South China Sea · South China Sea summer monsoon · Luzon strait transport · ENSO

1 Introduction

The South China Sea (SCS) is a semi-enclosed marginal sea in the tropical western Pacific Ocean, and it connects to the East China Sea, the Pacific Ocean, the Sulu Sea and the Java

Sea mainly through Taiwan Strait, Luzon Strait, Mindoro Strait and Karimata Strait, respectively. Under the influence of the East Asian Monsoon, the basin scale upper layer circulation in the SCS is cyclonic in winter and anticyclonic in summer, basically follows the wind-forced Rossby wave mechanism (Wyrtki 1961; Liu et al. 2001, 2008). The most prominent features of the summer upper layer circulation are the eastward offshore jet around 12°N against the Vietnam coast and the associated dipole structures (Metzger and Hurlburt 1996; Fang et al. 1998; Wu et al. 1998; Fang et al. 2002; Wang et al. 2006c). The eastward jet is also called the Vietnam Coastal Current, and the dipole structure is also phrased as double gyre or eddy pair in some literatures. The upwelling and advection accompanied by the summer circulation causes an obvious semiannual cycle and interannual variation of the sea surface temperature (SST) (Xie et al. 2003; Wang et al. 2006a), influences the upper layer thermal structure (Chen et al. 2010), reduces the local wind speed at the sea surface and enhances the air-sea interaction (Xie et al. 2007), and affects chlorophyll-a concentrations

Electronic supplementary material The online version of this article (<https://doi.org/10.1007/s00382-019-05007-5>) contains supplementary material, which is available to authorized users.

✉ Dongxiao Wang
dxwang@scsio.ac.cn

¹ State Key Laboratory of Tropical Oceanography, South China Sea Institute of Oceanology, Chinese Academy of Sciences, Guangzhou, People's Republic of China

² Guangzhou Branch, Southern Marine Science and Engineering Guangdong Laboratory (Guangzhou), Guangzhou, People's Republic of China

³ School of Atmospheric Sciences, Sun Yat-Sen University, Guangzhou, People's Republic of China

(Kuo et al. 2000; Tang et al. 2004; Liu et al. 2012; Chen et al. 2014). Thus, extensive researches have been carried out to study the formation and variability of the SCS summer circulation, because of its pronounced effects on the oceanic and atmospheric environment.

The formation of the eastward jet and dipole structure is mainly due to the orographic local wind stress curl by Annam mountain in Vietnam (Xu et al. 2008), and their variations are sensitive to the strength, direction and zonal asymmetry of the wind jet in an idealized rectangle basin (Wang et al. 2006c). While considering realistic topography, the interaction between wind-driven coastal currents and coastal promontory is another key factor, instead of wind stress curl alone, that controls the coastal jet separation around Vietnam at 12°N (Gan and Qu 2008). According to the western boundary current separation formula of Marshall and Tansley (2001), the critical separation velocity in this region is 0.29 m/s, which only occurs during strong southwesterly summer monsoon (Dippner et al. 2013). Besides local wind and topography, the encounter of two buoyancy-driven coastal current and tidal-rectification near Vietnam coast might also be favorable factors for the offshore current separation (Chen et al. 2012), and nonlinear advection would affect the strength and separation location of the current (Cai et al. 2007) as well.

The eastward jet also shows distinct variability from intra-seasonal to inter-decadal time scale, because of its sensitivity to the SCS summer monsoon. Each year, the development of the jet usually experiences 2–3 intra-seasonal cycles instead of simply persists through the summer monsoon, which is possibly owing to its response to Madden–Julian Oscillation (Xie et al. 2007). On interannual time scale, the stronger/weaker and southward/northward migration of the eastward jet at the developing/decaying stage of an El Niño event and the disappearance of the eddy pair during the strong El Niño to La Niña transition year are found to be mainly related to the southwesterly/northeasterly anomaly of the SCS summer monsoon (Chen and Wang 2014; Li et al. 2014; Chu et al. 2017), while the oceanic internal variability (such as the eddy-mean flow interaction) is found to be less important (Yang et al. 2015) and is estimated to contribute about 20% of the variation (Li et al. 2014). The inter-decadal variability of the eastward jet is closely related to the pattern and strength of the Asian summer monsoon (Wang et al. 2010) modulated by Pacific Decadal Oscillation (PDO) and Atlantic multidecadal oscillation (AMO) (Fang et al. 2014; Fan et al. 2018), and it is also influenced by the remote signals via Kelvin waves from the Western tropical Pacific through Sulu Sea (Fang et al. 2014).

Nevertheless, most previous studies focused on the role of wind on the change of the SCS upper layer circulation in summer, and there were few discussions on the contribution of Luzon strait transport (LST) (i.e. South China

Sea Through Flow, SCSTF), despite that its variation is closely related to ENSO and PDO (Qu et al. 2004; Wang et al. 2006b; Yu and Qu 2013). Recent studies show that the LST is equally important compared to the local wind for the formation of the SCS western boundary current (SCSWBC) (Chen and Xue 2014), and the interannual variation of SCSWBC is related to the LST (Quan et al. 2016). Moreover, the advection of planetary vorticity through lateral boundaries (mainly through Luzon strait) is found to be an important vorticity source of the upper layer cyclonic circulation, especially for the northern SCS (NSCS) in summer (Gan et al. 2016; Zhu et al. 2017; Quan and Xue 2018). The lateral boundary forcing is shown to have greater influence on the cyclonic circulation in summer than that in winter (Chu et al. 1999; Gan et al. 2016). Thus, when the change of Kuroshio intrusion and LST contributes obviously to the intensified interannual variation of the circulation in the southern SCS (SSCS) in winter through SCSWBC advection (Zu et al. 2019), we would suggest that it will also influence the interannual variation of the SCS upper layer circulation in summer.

It is known that SCS summer monsoon (SCSSM) (Wang et al. 2009; Zhou and Chan 2007) and the LST (Qu et al. 2004; Wang et al. 2006b) are greatly modulated by the El Niño–Southern Oscillation (ENSO), and the interannual variation of the summer circulation is significantly influenced by the SCSSM (Chen and Wang 2014; Li et al. 2014; Chu et al. 2017), but whether the LST plays an important role and how much contribution it does to the interannual change of the SCS summer circulation remains largely unclear.

In this paper, the characteristics of interannual variation of the summer circulation are re-explored, a prominent anti-correlation between an eastward jet (eastward branch: EB for short) and a northward branch (NB for short) along the western boundary is revealed, and their variation with the SCS summer monsoon and LST are discussed. The remainder of the paper is organized as follows. Section 2 gives a description on the data and model utilized, Sect. 3 shows the interannual variation of the summer circulation, Sect. 4 explores the relative contribution of local wind and lateral boundary advection and their responses to ENSO complexity, Sect. 5 summarize the findings.

2 Data and model

2.1 Data

Two types of observed current data are used to study the interannual variation of the summer circulation in the SCS. One is surface geostrophic current derived from $1/4 \times 1/4^\circ$ gridded daily sea surface height (SSH) data over 20 years (1993–2016). The SSH data is merged from

multi-altimetry products of TOPEX/Poseidon (T/P), Jason-1, Jason-2, ENVISAT, GFO, and ERS-1/2, with tidal corrections and mean dynamic topography added [provided by the Archiving, Validation, and Interpretation of Satellite Oceanographic data (AVISO)]. And the surface geostrophic currents are calculated using the horizontal gradients of SSH as the following,

$$(u_g, v_g) = \frac{g}{f} \left(-\frac{\partial SSH}{\partial y}, \frac{\partial SSH}{\partial x} \right) \quad (1)$$

in which g is the gravitational acceleration, and f is the Coriolis parameter.

The other type of current data is velocity profile obtained from two Acoustic Doppler Current Profilers (ADCP) mooring stations from 2007 to 2016. One of the station is located in the NSCS (at 110.3°E, 17.1°N) on the path of northern branch of the western boundary current, and the other one is in the SSCS basin (at 113°E, 9.7°N) on the path of the eastward jet. The velocities from the moorings are smoothed by using a window of 30-days to remove high frequency oscillations. The velocity from mooring station in NSCS reveals the year to year variability of the SCSWBC current, especially in the summer (Shu et al. 2016). By comparing the simultaneous observation from the mooring station in the SSCS, we find an anti-correlated interannual variation between these two stations, indicating a competitive relationship between the NB and EB in summer.

The $1/4 \times 1/4^\circ$, daily averaged wind field at 10 m from the Cross-Calibrated Multi-Platform (CCMP) ocean surface wind product (Atlas et al. 2011), and three dimensional daily current product of Hybrid Coordinate Ocean Model + Navy Coupled Ocean Data Assimilation (HYCOM + NCODA) global $1/12^\circ$ Analysis (GLBu0.08, <http://www.hycom.org/dataserver/gofs-3pt0/reanalysis>) are used in this study to explore the effects of local wind and LST on the interannual variation of the summer circulation.

2.2 Model

The Advanced Taiwan Ocean Prediction (ATOP) model (Oey et al. 2013) is utilized in this paper to explore the influence of LST to the anti-correlated interannual variation of the EB and NB. ATOP is developed from Princeton Ocean Model (POM), which covers the entire North Pacific Ocean and SCS, with a horizontal resolution of $0.1^\circ \times 0.1^\circ$ and 41 vertical sigma levels. It has been successfully used to study the interaction between the SCS through flow (SCSTF) and the Indonesian through flow (ITF) (Wei et al. 2016; Li et al. 2019), and detailed description of the model setup could be found in Oey et al. (2013).

To evaluate the effects from LST, numerical sensitivity experiment by closing the LS was carried out. The

sensitivity experiments were restarted from Jan. 2004 and run for additional 8 years, and the monthly mean results of July and August in 2009 and 2010 are utilized for analysis.

3 Result

3.1 General feature of the summer circulation

The monthly climatology mean surface geostrophic currents and wind stress curl from June to September (Fig. 1) show the general evolution of the summer circulation in response to the summer monsoon in the SCS. After the break of the SCS summer monsoon in May, a northward flow is formed along the western boundary of the SCS in May. The magnitude of the flow increases from June to August as the SCS summer monsoon is enhanced, and an eastward jet forms around 12°N against the Vietnam coast and becomes stronger since July. In September, when the southwesterly summer monsoon starts to change into northeasterly winter monsoon in the NSCS, the circulation pattern varies with that from June to August. The flow along the west boundary in the NSCS turns to southward or southwestward, and a well-developed cyclonic circulation appears north to the eastward jet. Together with the anticyclonic circulation south of it, they form the dipole structures. Similarly, the monthly climatology temperature and salinity (data from SCSP0D15, Zeng et al. 2016) at 30 m depth in September also show different structure with those from June to August. There is colder and saltier upwelling water along the western boundary north of 11°N near Vietnam coast from June to August, but an obvious dipole structure in September, with colder and saltier core in the north, and warmer and fresher core in the south of the eastward jet. Thus, the average of the circulation in July and August are used to represent the mature pattern of the SCS summer circulation in this paper.

3.2 Variability of the summer circulation

The climatology of the mature pattern of summer circulation, averaged by the monthly mean surface geostrophic current of July and August from 1993 to 2016, shows clearly a bifurcation of the current near the Vietnam coast, with a strong eastward jet separating from the northward boundary current and a weaker branch continuing flowing northward (Fig. 2a). A part of the eastward jet flows southward as an anticyclonic recirculation that joins the WBC in the SSCS. There are two strong negative vorticity cores in the anticyclonic circulation in the SSCS, while there is no evident cyclonic circulation or positive vorticity core to the north of the eastward jet. The first EOF mode of the summer surface kinetic energy (Fig. 2b) and velocity speed (supporting information Fig. S1) both show distinct competition between

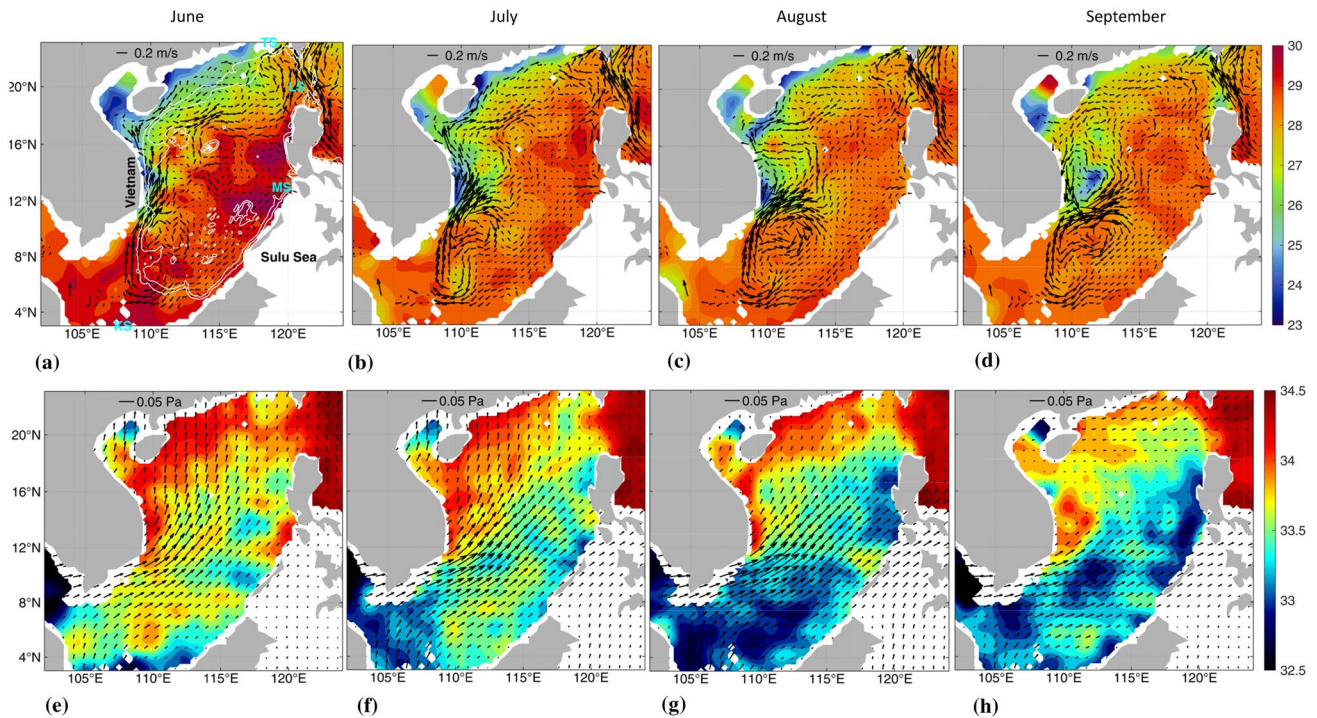


Fig. 1 Monthly climatology temperature (upper row in color shading: °C) at 30 m depth, superimposed with monthly climatology surface geostrophic current (current in the SCS basin where water depth is shallower than 75 m is not shown, vectors: m/s) and monthly climatology salinity (lower row in color shading) at 30 m depth, superimposed with monthly climatology wind stress at 10 m height from June to September. The temperature and salinity data is from SCSPD15,

which is obtained by merging Argo float, WOD94 and cruise observations. The surface geostrophic currents are obtained from AVISO. The wind stress is obtained from CCMP. TS, LS, MS, and KS in a stand for Taiwan Strait, Luzon Strait, Mindoro Strait, and Karimata Strait respectively. The white lines in **a** indicate the -200 and -1000 m isobaths

the NB and EB (eastward jet), and they account for 28.5% and 22.5% of the total variance, respectively. This pattern indicates that when the NB is enhanced, the EB and anticyclonic circulation in the SSCS is weakened, and vice versa. Besides, it also implies that the variation of the boundary current along the western SCS in summer is mainly regulated by the competitive bifurcation of the WBC against the Vietnam coast around 12°N . Likewise, the first EOF mode of the summer surface velocity speed from HYCOM simulation GLBu0.08 show similar pattern as those derived from AVISO, and it accounts for about 28% of the total variance (Fig. 6c). The anti-correlation of the strength of the NB and EB is also clearly observed from the spatial correlation of their mean speed with the whole SCS region (supporting information Fig. S1).

The temporal coefficient of the first EOF mode (PC1) of the summer surface kinetic energy shows correlation with the Nino3.4 index (Fig. 2c). They have better negative correlation at strong ENSO cycles (i.e. an El Niño event followed by a La Niña event in 1994–1995, 1997–1998, 2009–2010), which suggests that the EB is enhanced during El Niño developing phase, while the NB is enhanced during El Niño decaying and La Niña developing phase.

Previous results also pointed out a stronger/weaker and southward/northward movement of the eastward jet during developing/decaying stage of an El Niño event (Chen and Wang 2014; Li et al. 2014), or even disappeared in transition summer from strong El Niño to La Niña, such as in 2010 (Chu et al. 2017). However, the PC1 does not show clear relationship with the Nino3.4 at the second El Niño or La Niña developing phase during multiyear El Niño or La Niña events (i.e. 1999, 2011, 2015). This suggests that strong ENSO signals play important roles on the interannual correlation of the eastward and northward branches of the summer circulation, but the year to year variations of summer circulation are not solely influenced by ENSO. Li et al. (2014) and Yang et al. (2015) pointed out that besides southwesterly summer monsoon, ocean internal variability also contributes to the variation of the eastward jet, and this together with other factors will be further discussed in Sect. 4.

The anti-correlated interannual variations of the EB and NB are also demonstrated by the current observations from ADCP mooring station N and S (their locations are shown in Fig. 2a). Station N is on the path of western boundary current in the NSCS, the positive along-isobath

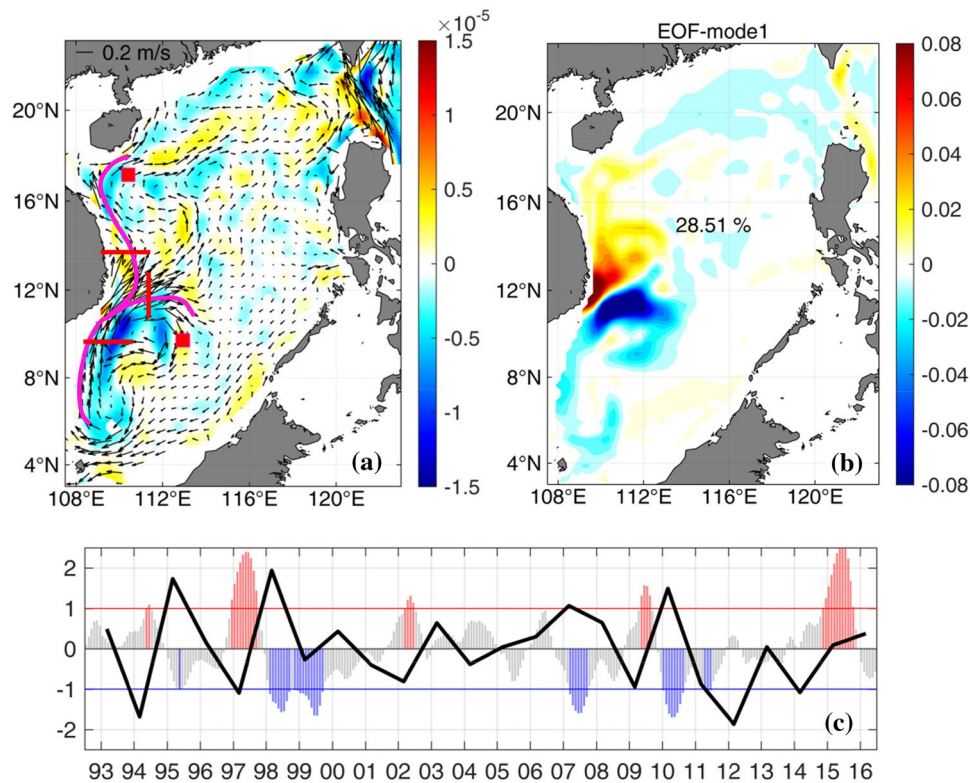


Fig. 2 **a** Climatology surface geostrophic current (vectors: m/s) and related vorticity (color shading: s^{-1}) in summer, **b** the first EOF mode of summer surface kinetic energy per unit mass, and it accounts for 28.51% of the total variance, **c** the normalized temporal coefficient of the first EOF mode (PC-1: black lines) superimposed on Nino3.4 index, x-axis is the summer of each year. The red bars indicate index greater than 1 and the blue bars indicate the index less than -1 . In **a** and **b**, the surface geostrophic current and the first EOF mode of the summer surface kinetic energy in the SCS basin where water depth

is shallower than 75 m are not shown. The red squares in **a** show the locations of the two ADCP moorings in Fig. 3, and the red lines show the locations of the section for velocity transport along the pathways of the EB, NB and WBC in the SCS in Fig. 4. The pink lines in **a** depict the main branches (eastward and northward) of climatology surface geostrophic flow in summer. The mean summer flow and kinetic energy are obtained from the monthly surface geostrophic current from AVISO in July and August

velocity in station N represents northeastward flow while the negative value represents southwestward flow (left column in Fig. 3). Station S is on the path of the eastward jet in the SCS. The negative value indicates southward extension associated with the jet. At station N, a stronger northeastward flow exists in 2007, 2010, and 2013, vertically it ranges from surface to more than 300 m deep, and its magnitude could reach over 0.5 m/s at 50 m depth, while in 2009 and 2012, the northeastward flow is greatly weakened to less than 0.15 m/s or even changes to southwestward flow sometimes. On the contrary, at station S no obvious southward flow appears in 2007, 2010, and 2013, but strong southward flow occurs in 2009 and 2012 with magnitude greater than 0.5 m/s and depth less than 300 m. Thus, it is evident that when the NB is stronger, the EB is weaker, and vice versa. Summer mean surface geostrophic currents from AVISO, upper layer circulation from ATOP and HYCOM simulations in these years all show similar

anti-correlation between the EB and NB that is revealed by the ADCP mooring stations (supporting information Fig. S2–S4). Stronger NB appears in 2007, 2010 and 2013, while stronger EB and associated anticyclonic circulation in the SCS exists in 2009 and 2012. Although the N and S ADCP mooring stations are only two points, they are quite representative in demonstrating the variation of EB and NB, as they are located in the regions of significant difference between EB and NB (Fig. 5c).

Additionally, the relationship between the monthly mean velocity transport integrated for the upper 100 m at different sections (locations shown on Fig. 2a) along the pathways of the EB, NB and WBC also show a clear anti-correlation between the EB and NB, a positive correlation between the EB and WBC, while a weak negative correlation between the NB and WBC (Fig. 4). Their correlations suggest that this feature is partly related to the anticyclonic recirculation on the south of the EB,

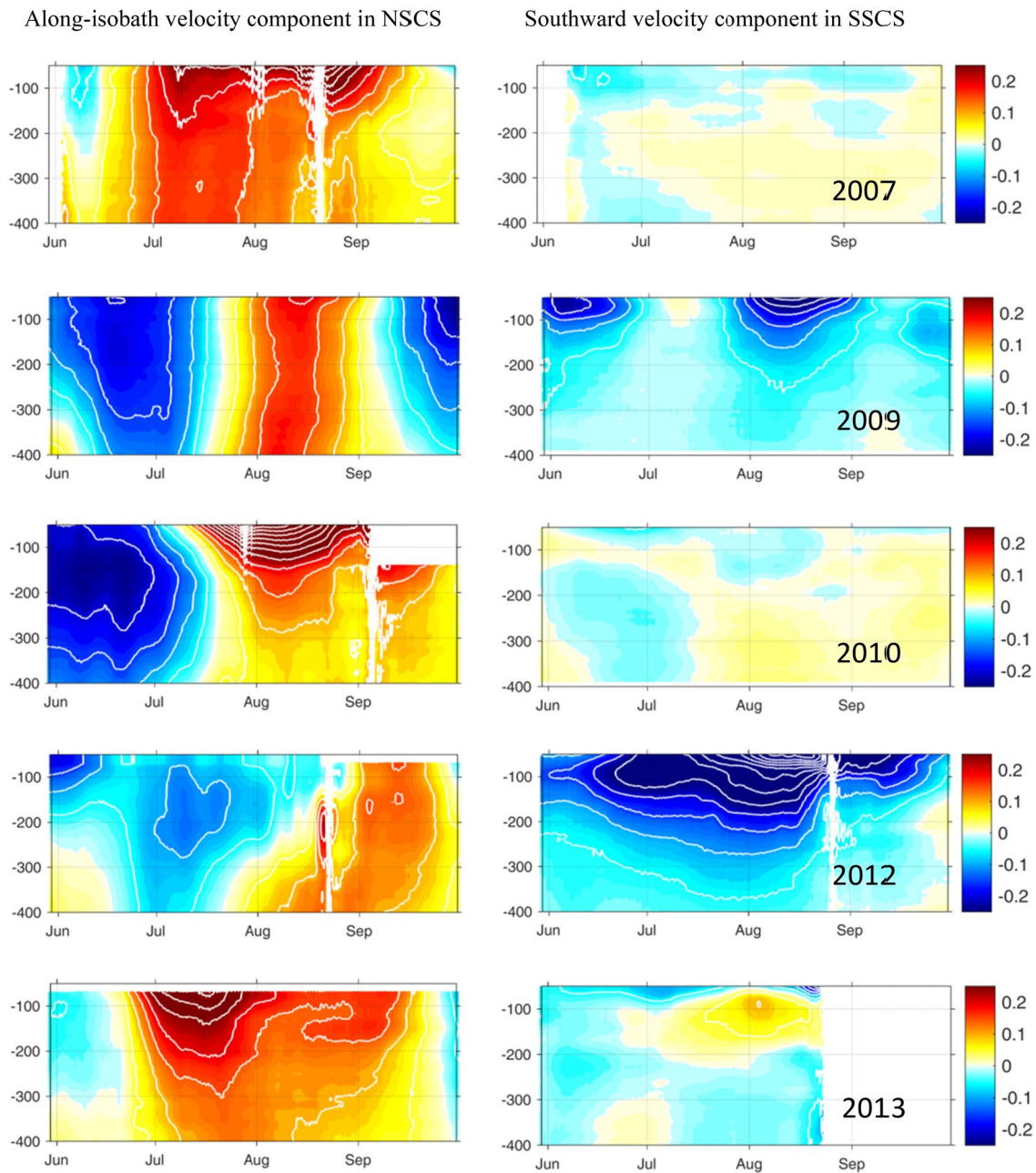


Fig. 3 Interannual variation of the along-isobath component (positive is northeastward) of the current (m/s, left column) observed at the ADCP mooring station N in the NSCS and the meridional component (positive is northward) of the current (m/s, right column) observed at the ADCP mooring station S in the SSCS. (The locations of the

stations are marked in Figs. 2a and 5c). The x-axis denotes the time from June to September. The y-axis is the water depth. The blank areas show the time and depth without observation. White contour lines indicate the velocity from -1 to 1 m/s at an interval of 0.05 m/s

which joins and reinforces the WBC and consequently the EB, thus keeps the negative vorticity in the SSCS and is not favorable of the formation of NB. Although strongly related with the EB, the NB is weakly correlated with the WBC, and this indicates that the NB is not only determined by its upstream strength, other processes, such as LST and eddy activities in the NSCS might affect it.

3.3 Composite patterns of eastward and northward flow

Surface geostrophic currents averaged in summer (July and August) in years with larger positive/negative value of normalized temporal coefficients of the first EOF mode (according to Fig. 2c) are selected for a composite analysis.

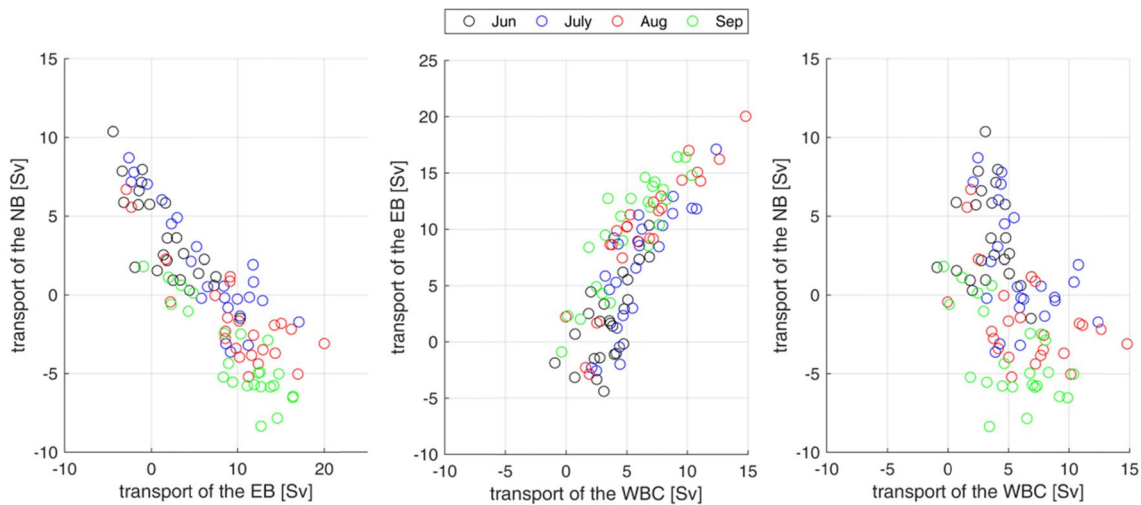


Fig. 4 Relationship between the monthly mean transports integrated at different sections for the current in the upper 100 m obtained from HYCOM GLBu0.08. **a** The transports of the northward branch and

the eastward branch, **b** the transports of the eastward branch and the WBC in the SCS, **c** the transports of the northward branch and the WBC in the SCS

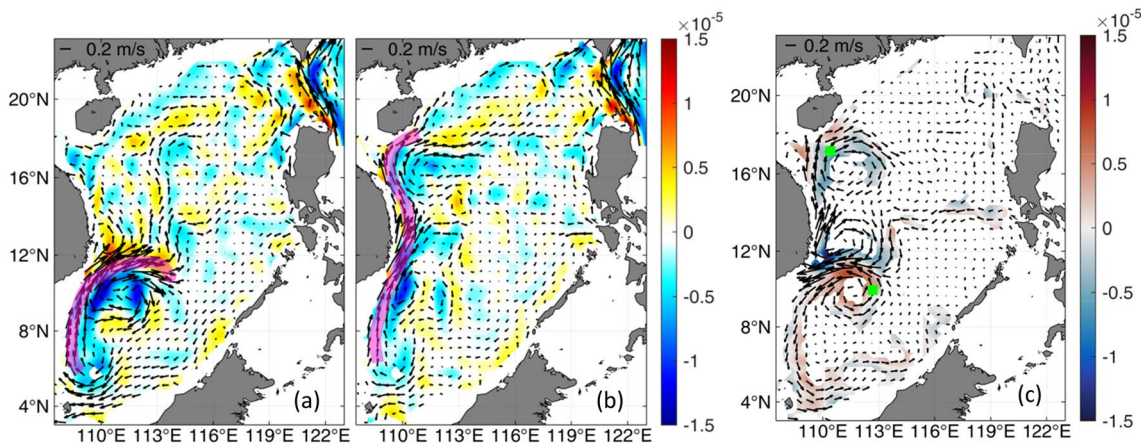


Fig. 5 Composite of the summer surface geostrophic current (vectors: m/s) and related vorticity (color contours: s^{-1}) derived from altimetry data from AVISO. **a** For eastward branch and **b** for northward branch. **c** The difference between the northward and eastward branch that past the *t*-test (shaded region). Eastward branch is the composite of currents in 1994, 1997, 2009, 2012, 2014, and northward branch is the

composite of currents in 1995, 1998, 2007, 2010. Selected years have large positive/negative values of the temporal coefficients of the first EOF mode of the KE as shown in Fig. 2c. Pink lines in **a** and **b** depict the major flow pattern in eastward and northward dominant patterns, respectively. The green squares in **c** show the locations of the two ADCP moorings in Fig. 3

Same years would be selected out for composite, if we use 1 standard deviation of the PC-1 as the threshold. Current composited by 1994, 1997, 2009, 2012, 2014 (with normalized PC-1 smaller than -1) show stronger EB (Fig. 5a), and those composited by 1995, 1998, 2007, 2010 (with normalized PC-1 larger than 1) show stronger NB (Fig. 5b). There is a prominent anticyclonic circulation in the SCS for the EB pattern, but no evident boundary current in the NSCS. However, for the NB pattern, a continuous western boundary current flowing from the southern basin to the northern shelf is obvious, and the eastward jet together with

the anticyclonic circulation in the southern basin are greatly weakened, instead a clear negative vorticity core appears around $16^{\circ}N$ in the NSCS. The differences between EB and NB (NB-EB) that past the *t* test (Fig. 5c) show a significant westward flow towards Vietnam coast between 11 and $12^{\circ}N$, with cyclonic circulations south of it, and anticyclonic ones north of it. The most prominent variation is along the western boundary of the SCS basin.

Composite currents from the HYCOM GLBu0.08 simulation also clearly show the EB and NB patterns at different depths from 0 to over 200 m below the surface (here, only

currents at 100 m depth are shown in Fig. 6). An anticyclonic circulation with strong eastward jet south of 12°N is the most prominent feature of the summer circulation in EB pattern, while a prolonged northward western boundary current from 8 to 18°N exists in NB pattern. The magnitude of the flow in NB is smaller than that in EB at the bifurcation region southwest of Vietnam.

4 Factors contributing to the interannual variation of the summer circulation

Early studies (e.g. Wyrki 1961; Shaw and Chao 1994) pointed out that monsoon wind is the dominant forcing for the seasonal variation of the upper layer circulation in the SCS, and thus a basin-scale anticyclonic circulation is the main feature in summer. Subsequent studies with more observations and higher resolution numerical models (Cai et al. 2002; Chern and Wang 2003; Chu et al. 1999; Fang et al. 1998; Gan et al. 2006; Hu et al. 2000; Qu et al. 2004; Wang et al. 2003, 2008; Xue et al. 2004; Yang et al. 2002) revealed the importance of the Kuroshio intrusion and LST on the complexity of the circulation in the NSCS, and some studies showed cyclonic circulation in the NSCS in summer. Recent studies (Gan et al. 2016; Zhu et al. 2017) suggested that the cyclonic upper layer circulation in the NSCS in summer is mainly induced by the advection of planetary vorticity through LST. And the influence from Kuroshio intrusion into the SCS is not limited in the NSCS, it could affect the circulation and water mass properties in the SSCS through western boundary current advection (Zu et al. 2019).

In Sect. 3, observations and numerical simulations all show that on interannual time scale, the summer SCS circulation could be sometimes a basin scale anticyclonic

circulation, and sometimes a strong anticyclonic circulation in the SSCS with either a weak cyclonic or anticyclonic circulation in the NSCS. In this section, we would further explore under what conditions will these patterns appear and the relative contributions of the SCS summer monsoon and LST to the variability of upper layer circulation in summer.

4.1 South China Sea summer monsoon

The spatial correlation between the kinetic energy of the summer surface circulation (derived from HYCOM GLBu0.08 current at 10 m depth) and the South China Sea summer monsoon index (SCSSMI) (Li and Zeng 2002) shows that a larger value exceeding the 90% confidence level is mainly along the western boundary current and the eastward jet (Fig. 7a). The SCSSMI is positively correlated to the southern segment of the western boundary current and the EB, while negatively correlated to the NB. This is similar to the first EOF mode of the surface velocity speed and kinetic energy that the NB and EB are anti-correlated (Figs. 2b, 6c and supporting information Fig. S1). It also indicates that when the South China Sea summer monsoon (SCSSM) is strengthened, the magnitude is increased for EB but decreased for NB, when the SCSSM is weakened, the contrary situation would appear. The temporal coefficient of first EOF mode (PC1) is negatively related with SCSSMI and the correlation coefficient is about -0.79 (Fig. 7e). When the influence of the LST is excluded, their partial correlation (Fig. 7c) shows similar spatial pattern as Fig. 7a, although the areas of the significant correlation is reduced. Greater difference between the results of the partial correlation and correlation mainly appears in the NB region, suggesting that SCSSM has larger impact on the eastward jet and related anticyclonic circulation in

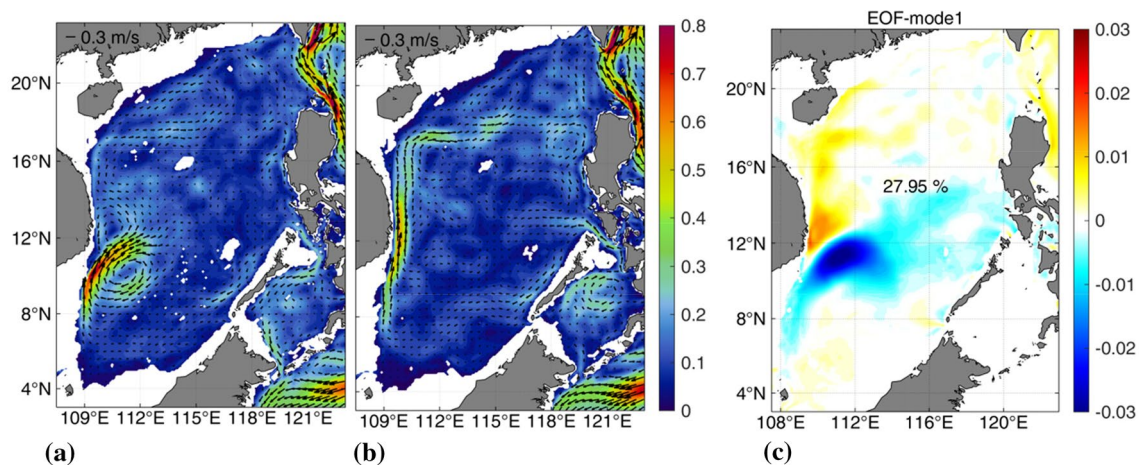
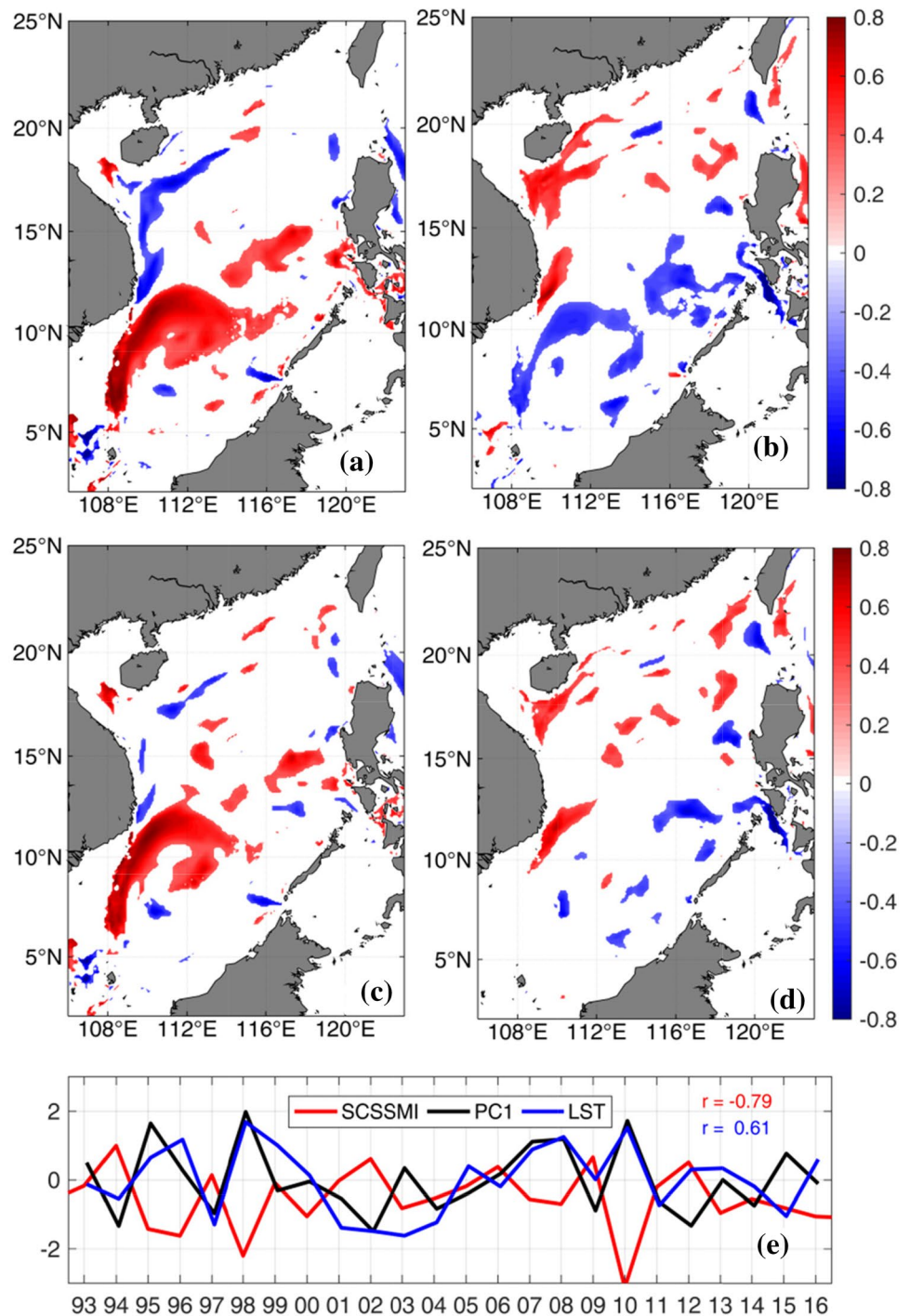


Fig. 6 Composite of the summer current (vectors: m/s) and current speed (color contours: m/s) at 100 m depth (a for eastward branch pattern and b for northward branch pattern) and the first EOF mode of summer surface velocity speed (c) from HYCOM simulation GLBu0.08

Fig. 7 Correlations (**a** and **b**) and partial correlations (**c** and **d**) of the South China Sea upper layer circulation between South China Sea summer monsoon index (SCSSMI) and the Luzon strait transport (LST). **a** Spatial distribution of correlation coefficients of the surface kinetic energy anomaly (current at 10 m depth derived from HYCOM GLBu0.08) between SCSSMI that exceeding the 90% confidence level. **b** Similar to **a** but for the anomaly of the surface kinetic energy and LST (derived from HYCOM GLBu0.08). **c** and **d** are similar to **a** and **b** but excluding the influences from LST and SCSSM, respectively. **e** Time series of the normalized temporal coefficient of the first EOF mode of the surface kinetic energy anomaly from HYCOM GLBu0.08 (PC1: black line), SCSSMI (red), and normalized LST (blue). The correlation coefficient between PC1 and SCSSMI is -0.79 and is 0.61 between PC1 and LST



the SSCS, whereas LST have larger impact on the northward branch of the WBC in the NSCS. Composites of the wind vectors and their vorticity in Fig. 8 show stronger southwesterly SCS summer monsoon in EB pattern, but a weaker one in NB pattern. In EB pattern years, a strong northeastward wind jet (6–8 m/s) is obvious between 9 and 15°N with positive vorticity in the north and negative vorticity in the south. Whereas, in NB pattern years, the

strength of the wind jet is greatly weakened (3–4 m/s) and the coverage of positive vorticity in the NSCS is reduced to a small region along the Vietnam coast. The difference of wind vectors between EB pattern and NB pattern (NB-EB) is a strong easterly anomaly from western tropic Pacific to the SCS and the Bay of Bengal (Fig. 8c), which suggest the strong influence from ENSO. The anomaly easterly wind jet in the SCS is around 9–10°N, and it also

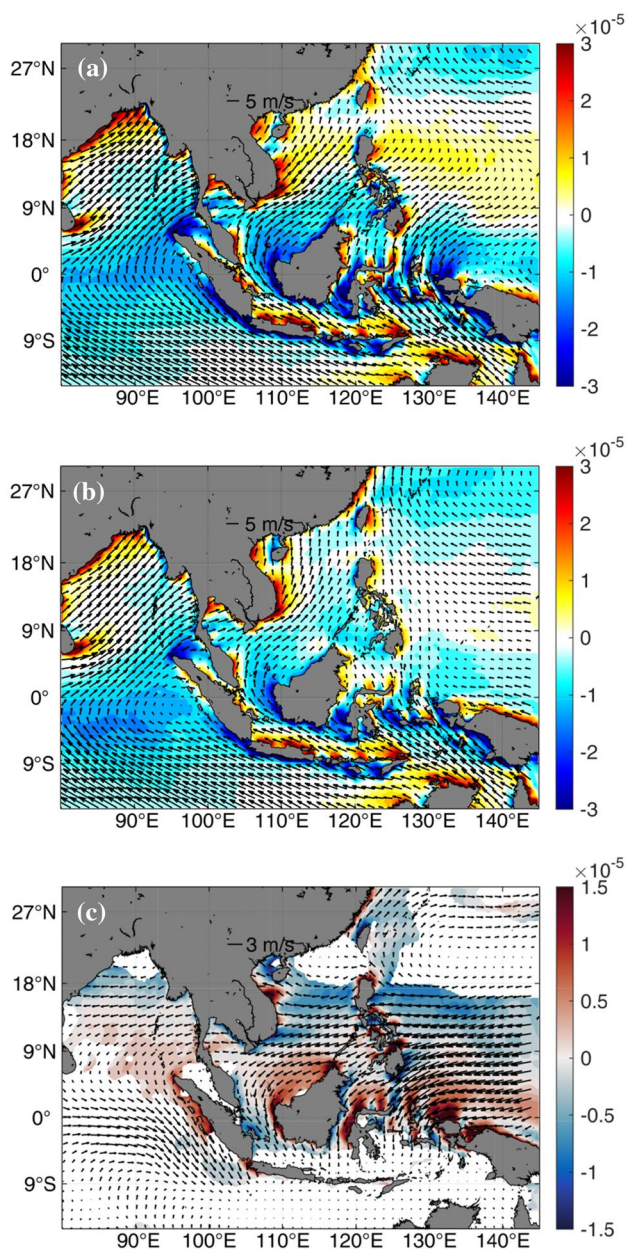


Fig. 8 Composite of the summer wind vectors (m/s) and related vorticity (s^{-1}) from CCMP data for **a** eastward branch, **b** northward branch. **c** The differences of wind vectors and vorticity between eastward and northward branch patterns (northward–eastward) that past the t-test (shaded region). Eastward branch is the composite of currents in 1994, 1997, 2009, 2012, 2014, and northward branch is the composite of currents in 1995, 1998, 2007, 2010

induces a negative curl in the NSCS and a positive curl in the SSCS, thus greatly weaken the EB and the anticyclonic circulation in the SSCS in the NB pattern years.

4.2 Luzon strait transport (SCSTF)

The spatial correlation between the SCS surface kinetic energy and the LST (both of them are derived from HYCOM GLBu0.08) in Fig. 7b also has larger and more significant correlation coefficient along the western boundary current and eastward jet. The LST (negative: net transport into the SCS, positive: net transport out of the SCS) is positively related to the NB, while negatively related to the EB and the southern segment of the western boundary current. It suggests that when the LST into the SCS increases, the eastward jet and the Mindoro Strait transport out of the SCS is enhanced (i.e. an increased SCSTF), whereas when the LST into the SCS decreases, the NB is enhanced and the EB is weakened. The LST is positively correlated with the PC1 (Fig. 7c), but the value of correlation coefficient is 0.61, smaller than that with SCSSMI. This implies that both SCSSM and the LST could affect the competitive interannual variation the EB and NB, and SCSSM might play a more important role than the LST. When the influence of the SCSSM is excluded, their partial correlation (Fig. 7d) shows similar spatial pattern as Fig. 7b, with the areas of the significant correlation being reduced. Major difference between the results of the partial correlation and correlation appears in the EB region and anticyclonic circulation region in the SSCS. This result again suggests that local wind stress curl has larger impact on the eastward jet and related anticyclonic circulation in the SSCS, whereas remote wind forcing and LST have larger impact on the northward branch of the WBC in the NSCS.

The LST and Mindoro Strait transport (MST) from April to October in EB and NB pattern years together with their composites in Fig. 9 show that the value of net LST into the SCS and the net MST out of the SCS (i.e. a branch of the SCSTF) are generally larger in EB years than in NB years. In July and August, the average difference could reach 3–4 Sv in both LS and MS. The greatest difference of about 6–7 Sv is between the extreme El Niño in 1997 and the extreme La Niña in 2010.

Sensitivity experiments by closing the Luzon Strait in ATOP simulation clearly show a weakened EB and associated double gyres in 2009, while an enhanced NB in 2010 (Fig. 10). It confirms that the net LST from Pacific into the SCS (advection of planetary vorticity) favors a tendency of cyclonic circulation in the NSCS, which would strengthen the EB but weaken the NB in summer.

4.3 Vorticity contribution from local wind stress and lateral flux

Besides the aforementioned comparisons, we have also made a quantitative estimate of the vorticity input from local wind stress curl and the advection of planetary vorticity fluxes

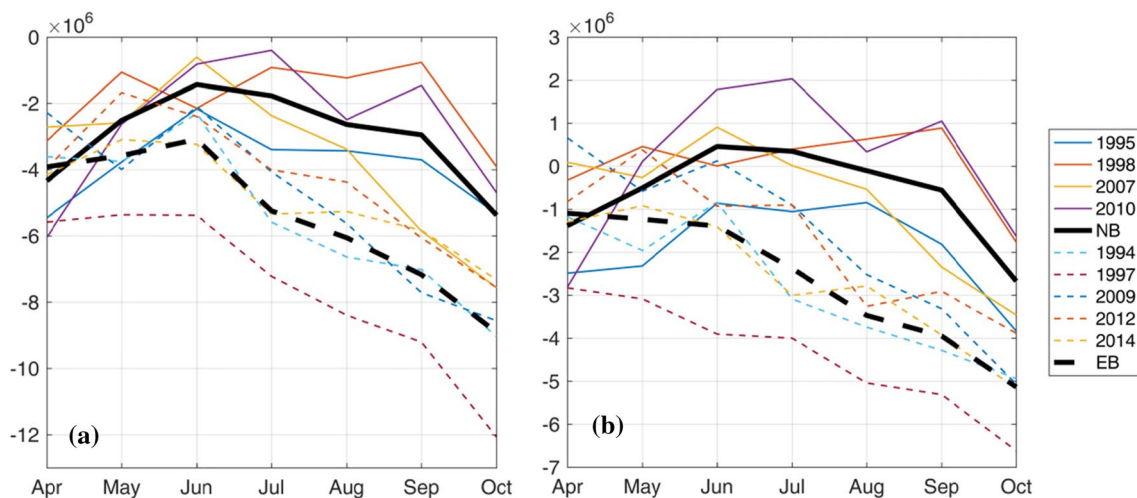


Fig. 9 Time series of the **a** Luzon strait, and the **b** Mindoro strait transports (m^3/s) from HYCOM simulation result GLBu0.08. The negative value of LST is into the SCS, while the negative value of MST is out of the SCS. Color lines are for different years, the blank

solid line indicates the composite of the northward branch years, and the black dash line indicates the composite of the eastward branch years

through the straits, as they are the major external vorticity sources for the cyclonic and anticyclonic seasonal circulations in the SCS (Xu and Oey 2014; Gan et al. 2016; Zhu et al. 2017; Quan and Xue 2018). In addition, the standard deviation of the vorticity of the surface geostrophic current in summer is larger in both magnitude and area next to the Vietnam coast along the western boundary of the SCS (supporting information Fig. S5). This indicates that the upper layer integrated vorticity variation in the SCS domain could well reflects the changes of vorticity and circulation in this region.

Domain and upper layer integrated vorticity budget Eq. (2) is written similar as that in Gan et al. (2016), Quan and Xue (2018).

$$\Omega_{ACC} + \Omega_{ADV} + \Omega_{COR} + \Omega_{PGF} + \Omega_{VVIS} + \Omega_{HDIF} = 0 \quad (2)$$

The terms in Eq. (2), from left to right are the curls of the acceleration Ω_{ACC} (tendency of relative vorticity), horizontal and vertical (vortex tilting) advection Ω_{ADV} , Coriolis force (vortex stretching) Ω_{COR} , pressure gradient force Ω_{PGF} , vertical viscosity Ω_{VVIS} and horizontal diffusion Ω_{HDIF} , respectively. After integration, in the upper layer, Ω_{VVIS} could be expressed as $\Omega_{VVIS} = \Omega_{USTR} + \Omega_{LSTR}$ (the sum of wind stress curl in the upper interface and frictional stress curl in the lower interface). The Coriolis force term could be written as $\Omega_{COR} = \oint U_n f dl$ (integral of planetary vorticity flux along the lateral boundary), where U_n is the vertically integrated velocity component perpendicular to the lateral boundary, and f is the Coriolis parameter.

Xu and Oey (2014), Gan et al. (2016), Zhu et al. (2017) and Quan and Xue (2018) all show that the major external vorticity input terms in the SCS upper layer circulation are

wind stress curl from atmosphere (Ω_{USTR}) and the lateral flux of the planetary vorticity from open-ocean through major straits (Ω_{COR}). In summer, both terms together balance the Ω_{PGF} , and other terms play minor roles on the balance (Quan and Xue 2018). Therefore, we only compare the contributions from these two terms. The Ω_{USTR} is calculated as the areal integration of the composite wind stress curl (Eq. (3)) in the region between 107–121°E and 3–25°N, where water depth is greater than 5 m.

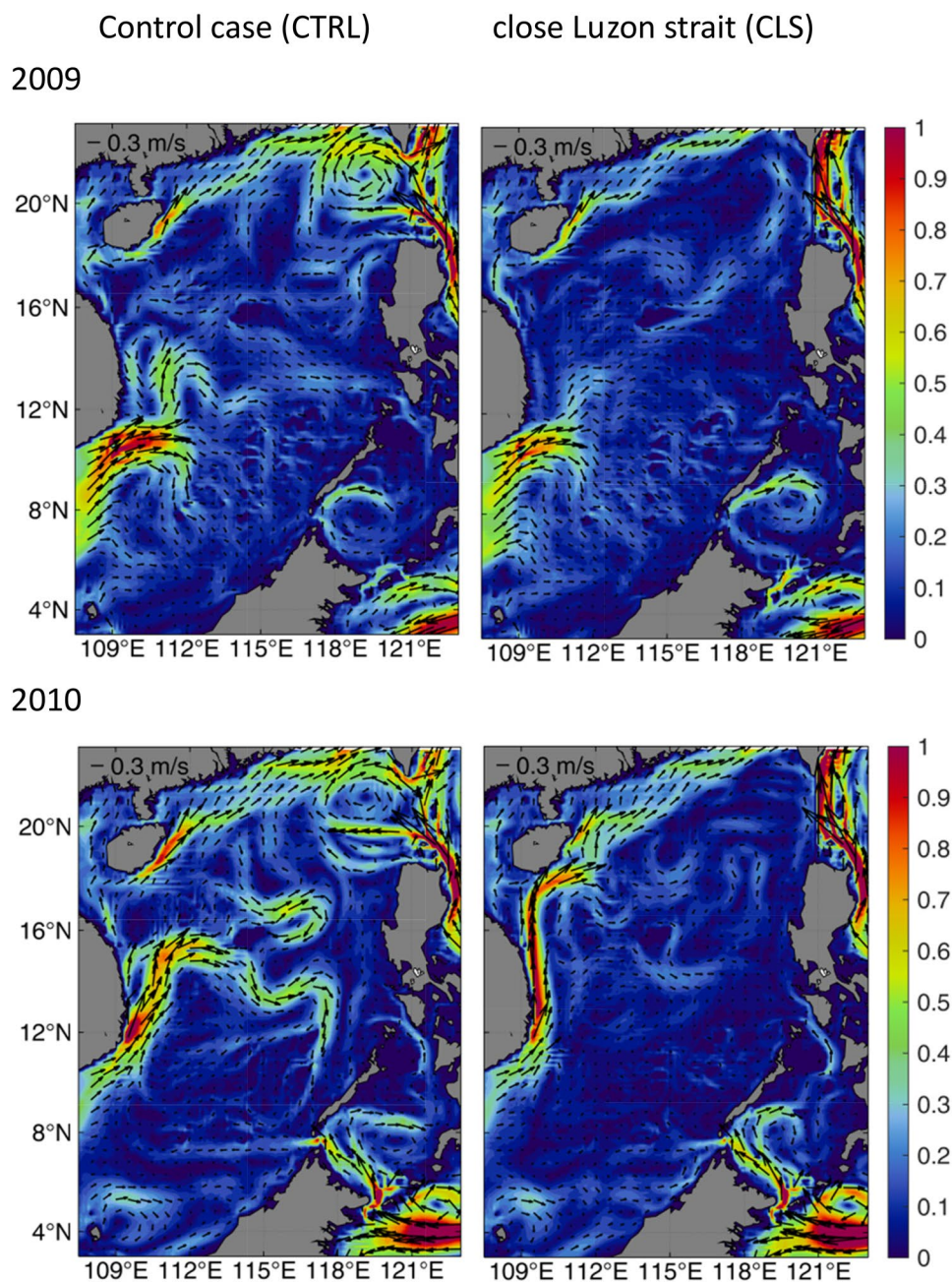
$$\Omega_{USTR} = \iint curl_z \left(\frac{\tau_a}{\rho_0} \right) dx dy \quad (3)$$

In which τ_a is wind stress, ρ_0 is the reference density of seawater, and the operator is defined as $curl_z(\vec{A}) = \frac{\partial A_y}{\partial x} - \frac{\partial A_x}{\partial y}$. The Ω_{COR} is calculated by the multiples of the composite transport and the Coriolis parameter f at the major straits.

$$\Omega_{COR} = \sum_{i=1}^N Q_i f_i \quad (4)$$

In which Q_i and f_i are the volume transport and Coriolis parameter at the i th strait. Karimata Strait is not considered here as the f is too small and consequently its contribution to the flux of the planetary vorticity is negligible. The roughly estimates of the relative contributions of these two terms are summarized in Table 1. In NB years, when the southwesterly summer monsoon is weakened, the magnitude of both positive and negative wind stress curl inputs into the SCS are smaller than those in EB years. But the net wind stress curl input of the whole SCS basin is about $-20 m^3 s^{-2}$ in NB years, which is twice of that in EB years.

Fig. 10 Surface current in July from ATOP control run (left column) and sensitivity case with Luzon Strait closed (right column) in 2009 and 2010. Color shading is the speed of the current (m/s)



The difference between NB and EB years (NB minus EB) is around $-10 \text{ m}^3 \text{ s}^{-2}$. The negative wind stress curl input favors an anticyclonic circulation in the SCS, thus the wind stress curl input contributes to a stronger anticyclonic circulation in the SSCS with eastward jet in EB years while a stronger NB and a basin scale anticyclonic circulation in NB years. Regarding to the flux of the planetary vorticity through the major straits (positive value means gaining positive vorticity, while negative value means losing positive vorticity), Luzon Strait (LS) transport favors cyclonic circulations, whereas Taiwan Strait (TS) transport favors anticyclonic circulations. Mindoro Strait (MS) transport

favors anticyclonic circulations in EB years, when the SSCS anticyclonic circulation and eastward jet are strong. The net flux of planetary vorticity is about $-73 \text{ m}^3 \text{ s}^{-2}$ in NB year, and $-56 \text{ m}^3 \text{ s}^{-2}$ in EB year. The difference between them is $-17 \text{ m}^3 \text{ s}^{-2}$, and it has a similar magnitude to the difference between the wind stress curl in NB and EB years. This suggests that the change of local wind stress and major strait transport contribute equally. Although the planetary vorticity flux at TS is large, on interannual variations, the change at LS is the major contributor to the negative difference of planetary vorticity flux between NB and EB years.

Table 1 Estimations of the domain integrated wind stress curl (WSC) and planetary vorticity flux through Luzon Strait (LS), Mindoro Strait (MS) and Taiwan Strait (TS) in the SCS in summer (July and August) of northward branch (NB) and eastward branch (EB) years. (Unit: $\text{m}^3 \text{s}^{-2}$)

	NB	EB	Diff (NB-EB)
WSC_P (positive)	42	96	-54
WSC_N (negative)	-62	-106	44
WSC (WSC_P + WSC_N)	-20	-10	-10
LS	50	143	-93
MS	3	-83	86
TS	-126	-116	-10
Net_flux (LS + MS + TS)	-73	-56	-17

4.4 Other factors that add to the complexity of the interannual variations

The interannual variation of the summer circulation in the SCS is influenced by the SCSSM and LST, which are modulated by the ENSO events. However, ENSO complexity might lead to complicated responses of the SCSSM and LST to ENSO events, and consequently a more complicated interannual variation of the summer circulation in the SCS. According to Yu and Fang (2018), there are ENSO cycles (one event followed by an opposite phase event), episodic events (one event preceded and followed by a neutral year), and multiyear El Niño or La Niña events. The charged-discharged (CD) mechanism tends to make regular and symmetric ENSO cycles, while seasonal footprinting (SF) mechanism tends to produce multiyear La Niña events and contributing to El Niño-La Niña asymmetries. From Fig. 2c, it is clear that during ENSO cycles (i.e. 1994–1995, 1997–1998, 2009–2010), there would always be obvious EB pattern in El Niño followed by strong NB pattern in La Niña. Nevertheless, the EB or NB pattern would not necessarily appear during episodic events (such as in 2002, 2007, 2015). Additionally, NB pattern will not appear in the second La Niña year during multiyear La Niña events (i.e. 1999, 2011). This suggests that the alternate appearance of the EB and NB pattern during ENSO cycles is a relatively deterministic response that is mainly related to the tropical ocean and atmosphere signals of CD mechanism, whereas the subtropical atmosphere–ocean coupled forcing of SF mechanism add uncertainty and complexity to the appearance of EB and NB patterns. However, to further understand the complexity of the appearance of the two kinds of circulation patterns, we need to explore the responses of the SCSSM and LST to the tropical and subtropical atmosphere–ocean coupled forcing, which is beyond the present work but deserves future efforts.

In addition to the ENSO complexity, ocean internal variability (OIV, through eddy-mean flow interactions) will also contribute to the interannual variation of the summer

circulation. Numerical experiments forced with monthly climatologic atmospheric fields show that the OIV accounts for about 20% of the interannual variability of the strength of the eastward jet and dipole structure at Vietnam coast (Li et al. 2014). When studying the interannual variation of the South Vietnam Upwelling (SVU), Da (2018) also shows that OIV could account for about 40% or even more of the observed interannual variation of the magnitude of the SVU, through numerical experiments with climatological daily atmospheric field and higher spatial resolution model. Both of them confirm the importance of OIV to the interannual complexity of the magnitude of the eastward jet and dipole structure and related upwelling. However, none of them shows visible influences of OIV on the displacements of the upwelling center or jet separating from the Vietnam coast. This implies again that interannual change of the local atmospheric fields and oceanic forcing play more significant roles on the variability of the major flow patterns in the SCS in summer.

5 Summary

By analyzing the current derived from altimetry data, ADCP moorings and numerical simulations, we revisited the interannual variation of the SCS upper layer circulation in summer, and provided another perspective (EB and NB patterns) to understand the change of the basin scale circulation in the SCS in summer. Besides the interannual variation of the eastward jet (EB) pointed out by many previous studies, we also revealed its anti-correlation with the NB. The results could be summarized by a sketch in Fig. 11. During El Niño developing phase, three major processes are in favor of a stronger EB: firstly, the stronger southwesterly summer monsoon with the zero wind stress curl across the SCS basin located more southward, is favorable for a separation of boundary current at a lower latitude, secondly, the stronger LST into the SCS with larger positive planetary vorticity flux is favorable for a cyclonic circulation in the NSCS which would facilitate boundary current separation and enhance the EB, thirdly, the recirculation associated with anticyclonic eddy on the south of the EB would strengthen the WBC and lead to a more robust EB. While during the El Niño decaying phase and La Niña developing phase, the situation is in favor of a NB pattern, a weaker summer monsoon with a northward and counter-clockwise shift of the zero wind stress curl line in the SCS basin is unfavorable for the boundary current separation, besides the decreased LST with greatly reduced positive planetary vorticity flux would not support for a cyclonic circulation in the NSCS. Basically, the shift between the EB and NB patterns is related to the interannual variation of the SCSSM and the LST. The contribution of the major strait transport to the interannual

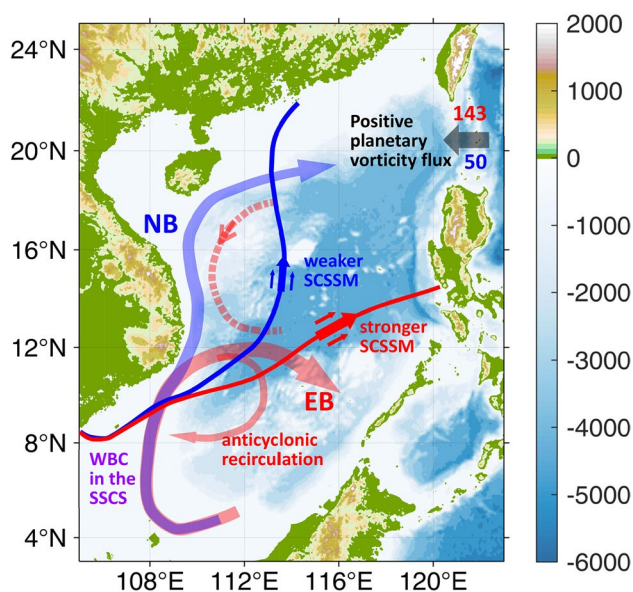


Fig. 11 Sketch of the two distinct patterns of the upper layer circulation in the SCS in summer superimposed on the topography map in this region. Red lines indicate the situation in EB pattern years, and blue lines indicate the situation in NB pattern year. The semitransparent solid lines show the main pathways of the circulation, and the semitransparent dash line shows the unstable flow or the tendency of the cyclonic circulation. The opaque lines indicate the zeros wind stress curl lines that across the SCS basin

variation of the SCS summer circulation is quantitatively evaluated for the first time, which show that the vorticity input from planetary vorticity flux through these major straits modulated by the remote wind forcing is as important as that from local wind stress curl. Moreover, results show that ENSO complexity also influences the interannual variation of the summer circulation. Further analysis of the responses of the SCSSM and LST to the ENSO complexity is needed to better understand and predict the interannual variation of the SCS summer circulation.

Acknowledgements We are grateful to the editor and two anonymous reviewers for their thoughtful comments and suggestions. We thank Gengxin Chen for his helpful discussion. We also thank the Advanced Taiwan Ocean Prediction model group (<http://mpipom.ihs.ncu.edu.tw>) to provide codes for the model simulations used in this study. We benefited from numerous data sets made freely available, including AVISO (<http://www.aviso.altimetry.fr/en/data/data-access.html>), CCMP (<http://www.remss.com/measurements/ccmp/>), HYCOM GLBu0.08 (<http://www.hycom.org/dataserver/gofs-3pt0/reanalysis>). This research was supported by the National Natural Science Foundation of China (NSFC) under Project (41521005, 41731173, 41576002, 41776026, 41576003), by No. GML2019ZD0304 from Southern Marine Science and Engineering Guangdong Laboratory (Guangzhou), and by the research fund from the State Key Laboratory of Tropical Oceanography (LTOZZ1803). Qiang Wang is also sponsored by the Pearl River S&T Nova Program of Guangzhou (201906010051).

References

- Atlas R et al (2011) A cross-calibrated, multiplatform ocean surface wind velocity product for meteorological and oceanographic applications. *Bull Am Meteorol Soc* 92:157–174
- Cai S, Su J, Gan Z, Liu Q (2002) The numerical study of the South China Sea upper circulation characteristics and its dynamic mechanism, in winter. *Cont Shelf Res* 22:2247–2264
- Cai S, Long X, Wang S (2007) A model study of the summer Southeast Vietnam Offshore Current in the southern South China Sea. *Cont Shelf Res* 27:2357–2372
- Chen C, Wang G (2014) Interannual variability of the eastward current in the western South China Sea associated with the summer Asian monsoon. *J Geophys Res.* <https://doi.org/10.1002/2014JC010309>
- Chen G, Xue H (2014) Westward intensification in marginal seas. *Ocean Dyn* 64:337–345
- Chen G, Hou Y, Zhang Q, Chu X (2010) The eddy pair off eastern Vietnam: interannual variability and impact on thermohaline structure. *Cont Shelf Res* 30:715–723
- Chen C, Lai Z, Beardsley RC, Xu Q, Lin H, Viet NT (2012) Current separation and upwelling over the southeast shelf of Vietnam in the South China Sea. *J Geophys Res* 117:C03033. <https://doi.org/10.1029/2011JC007150>
- Chen G, Xiu P, Chai F (2014) Physical and biological controls on the summer chlorophyll bloom to the east of Vietnam. *J Oceanogr* 70:323–328
- Chern C-S, Wang J (2003) Numerical study of the upper-layer circulation in the South China Sea. *J Oceanogr* 59:11–24
- Chu PC, Edmons NL, Fan C et al (1999) Dynamical mechanisms for the South China Sea seasonal circulation and thermohaline variabilities. *J Phys Oceanogr* 29(11):2971–2989
- Chu X, Dong C, Qi Y (2017) The influence of ENSO on an oceanic eddy pair in the South China Sea. *J Geophys Res* 122:1643–1652. <https://doi.org/10.1002/2016JC012642>
- Da Nguyen Dac (2018) The interannual variability of the South Vietnam Upwelling: contributions of atmospheric, oceanic, hydrologic forcing and the ocean intrinsic variability. *Ocean, Atmosphere.* Université Toulouse 3 Paul Sabatier (UT3 Paul Sabatier), 2018. English. <tel-01849114>
- Dippner JW, Bombar D, Loick-Wilde N, Voss M, Subramaniam A (2013) Comment on “Current separation and upwelling over the southeast shelf of Vietnam in the South China Sea” by Chen et al. *J Geophys Res* 118:1618–1623. <https://doi.org/10.1002/jgrc.20118>
- Fan Y, Fan K, Xu Z, Li S (2018) ENSO–South China Sea summer monsoon interaction modulated by the atlantic multidecadal oscillation. *J Clim* 31:3061–3076
- Fang G, Fang W, Fang Y, Wang K (1998) A survey of studies on the South China Sea upper ocean circulation. *Acta Oceanogr Taiwanica* 37(1):1–16
- Fang WD, Fang GH, Shi P, Huang QZ, Xie Q (2002) Seasonal structures of upper layer circulation in the southern South China Sea from in situ observations. *J Geophys Res* 107(C11):3202. <https://doi.org/10.1029/2002JC001343>
- Fang W, Qiu F, Guo P (2014) Summer circulation variability in the South China Sea during 2006–2010. *J Mar Syst* 137:47–54
- Gan J, Qu T (2008) Coastal jet separation and associated flow variability in the southwest South China Sea. *Deep-Sea Res* 55:1–19
- Gan J, Li H, Curchitser EN, Haidvogel DB (2006) Modeling South China Sea circulation: response to seasonal forcing regimes. *J Geophys Res* 111:C06034. <https://doi.org/10.1029/2005jc003298>
- Gan J, Liu Z, Hui C (2016) A three-layer alternating spinning circulation in the South China Sea. *J Phys Oceanogr* 46:2309–2315. <https://doi.org/10.1175/JPO-D-16-0044.1>
- Hu J, Kawamura H, Hong H, Qi Y (2000) A review on the currents in the South China Sea: seasonal circulation South China Sea Warm Current and Kuroshio intrusion. *J Oceanogr* 56:607–624

- Kuo NJ, Zheng Q, Ho CR (2000) Satellite observation of upwelling along the western coast of the South China Sea. *Remote Sens Environ* 74:463–470
- Li JP, Zeng QC (2002) A unified monsoon index. *Geophys Res Lett* 29(8):1274. <https://doi.org/10.1029/2001GL013874>
- Li Y, Han W, Wilkin JL, Zhang WG, Arango H, Zavala-Garay J, Levin J, Castruccio FS (2014) Interannual variability of the surface summertime eastward jet in the South China Sea. *J Geophys Res* 119:7205–7228. <https://doi.org/10.1002/2014JC010206>
- Li M, Wei J, Wang D, Gordon AL, Yang S, Malanotte-Rizzoli P, Jiang G (2019) Exploring the importance of the Mindoro-Sibutu pathway on the upper layer circulation of the South China Sea and the Indonesian throughflow. *J Geophys Res* 124:5054–5066. <https://doi.org/10.1029/2018JC014910>
- Liu Z, Yang HJ, Liu QY (2001) Regional dynamics of seasonal variability of sea surface height in the South China Sea. *J Phys Oceanogr* 31(1):272–284
- Liu QY, Kaneko A, Su JL (2008) Recent progress in studies of the South China Sea circulation. *J Oceanogr* 64(5):753–762. <https://doi.org/10.1007/s10872-008-0063-8>
- Liu X, Wang J, Cheng X, Du Y (2012) Abnormal upwelling and chlorophyll-a concentration off South Vietnam in summer 2007. *J Geophys Res* 117:C07021. <https://doi.org/10.1029/2012JC008052>
- Marshall DP, Tansley CE (2001) An implicit formula for boundary current separation. *J Phys Oceanogr* 31:1633–1638
- Metzger EJ, Hurlburt HE (1996) Coupled dynamics of the South China Sea, the Sulu Sea and the Pacific Ocean. *J Geophys Res* 101:12331–12352
- Oey LY, Chang YL, Lin YC, Chang MC, Xu F, Lu HF (2013) ATOP—advanced Taiwan ocean prediction system based on the mpiPOM: Part I: model descriptions, analyses and results. *Terr Atmos Ocean Sci* 24(1):137–158
- Qu T, Kim YY, Yaremchuk M, Tozuka T, Ishida A, Yamagata T (2004) Can Luzon strait transport play a role in conveying the impact of ENSO to the South China Sea? *J Clim* 17:3644–3657
- Quan Q, Xue H (2018) Layered model and insights into the vertical coupling of the South China Sea circulation in the upper and middle layers. *Ocean Model* 129:75–92
- Quan Q, Xue H, Qin H, Zeng X, Peng S (2016) Features and variability of the South China Sea western boundary current from 1992 to 2011. *Ocean Dyn* 66:795–810
- Shaw P-T, Chao S-Y (1994) Surface circulation in the South China Sea. *Deep-Sea Res* 41(1):1663–1683
- Shu Y, Xue H, Wang D, Xie Q, Chen J, Li J, Chen R, He Y, Li D (2016) Observed evidence of the anomalous South China Sea western boundary current during the summers of 2010 and 2011. *J Geophys Res* 121:1145–1159. <https://doi.org/10.1002/2015JC011434>
- Tang DL, Kawamura H, Doan-Nhu H, Takahashi W (2004) Remote sensing oceanography of a harmful algal bloom off the coast of southeastern Vietnam. *J Geophys Res* 109:C03014. <https://doi.org/10.1029/2003JC002045>
- Wang G, Su J, Chu PC (2003) Mesoscale eddies in the South China Sea observed with altimeter data. *Geophys Res Lett* 30(21):2121. <https://doi.org/10.1029/2003GL018532>
- Wang C, Wang W, Wang D, Wang Q (2006a) Interannual variability of the South China Sea associated with El Niño. *J Geophys Res* 111:C03023. <https://doi.org/10.1029/2005JC003333>
- Wang D, Liu Q, Huang RX, Du Y, Qu T (2006b) Interannual variability of the South China Sea throughflow inferred from wind data and an ocean data assimilation product. *Geophys Res Lett* 33:L14605. <https://doi.org/10.1029/2006GL026316>
- Wang G, Chen D, Su J (2006c) Generation and life cycle of the dipole in the South China Sea summer circulation. *J Geophys Res* 111:C06002. <https://doi.org/10.1029/2005JC003314>
- Wang D, Xu H, Lin J, Hu J (2008) Anticyclonic eddies in the north-eastern South China Sea during winter 2003/2004. *J Oceanogr* 64:925–935. <https://doi.org/10.1007/s10872-008-0076-3>
- Wang B, Huang F, Wu Z, Yang J, Fu X, Kikuchi K (2009) Multi-scale climate variability of the South China Sea monsoon: a review. *Dyn Atmos Oceans* 47:15–37
- Wang G, Wang C, Huang RX (2010) Interdecadal variability of the eastward current in the South China Sea associated with the summer Asian monsoon. *J Clim* 23:6115–6123
- Wei J, Malanotte-Rizzoli P, Li M, Wang D (2016) Opposite variability of Indonesian throughflow and South China Sea throughflow in the Sulawesi Sea. *J Phys Oceanogr*. <https://doi.org/10.1175/JPO-D-16-0132.1>
- Wu CR, Shaw PT, Chao SY (1998) Seasonal and interannual variations in the velocity field of the South China Sea. *J Oceanogr* 54:361–372
- Wyrtki K (1961) Scientific results of marine investigations of the South China Sea and the Gulf of Thailand 1959–1961. Naga Report, vol 2, University of California at San Diego, pp 164–169
- Xie SP, Xie Q, Wang D, Liu WT (2003) Summer upwelling in the South China Sea and its role in regional climate variations. *J Geophys Res* 108(C8):3261. <https://doi.org/10.1029/2003JC001867>
- Xie SP, Chang CH, Xie Q, Wang D (2007) Intraseasonal variability in the summer South China Sea: wind jet, cold filament, and recirculations. *J Geophys Res* 112:C10008. <https://doi.org/10.1029/2007JC004238>
- Xu FH, Oey LY (2014) State analysis using the local ensemble transform Kalman filter (LETKF) and the three-layer circulation structure of the Luzon Strait and the South China Sea. *Ocean Dyn* 64(6):905–923
- Xu H, Xie SP, Wang Y, Zhuang W, Wang D (2008) Orographic effects on South China Sea summer climate. *Meteorol Atmos Phys* 100:275–289
- Xue H, Chai F, Pettigrew N, Xu D, Shi M, Xu J (2004) Kuroshio intrusion and the circulation in the South China Sea. *J Geophys Res*. <https://doi.org/10.1029/2002jc001724>
- Yang H, Liu Q, Liu Z, Wang D, Liu X (2002) A general circulation model study of the dynamics of the upper ocean circulation of the South China Sea. *J Geophys Res* 107(C7):3085
- Yang H, Wu L, Shantong S, Zhaohui C (2015) Low-frequency variability of monsoon-driven circulation with application to the south China sea. *J Phys Oceanogr* 45(6):1632–1650
- Yu JY, Fang SW (2018) The distinct contributions of the seasonal footprinting and charged-discharged mechanisms to ENSO complexity. *Geophys Res Lett*. <https://doi.org/10.1029/2018GL077664>
- Yu K, Qu T (2013) Imprint of the Pacific decadal oscillation on the South China Sea throughflow variability. *J Clim* 26:9797–9805. <https://doi.org/10.1175/JCLI-D-12-00785.1>
- Zeng L, Wang D, Chen J, Wang W, Chen R (2016) SCSP0D14, a South China Sea physical oceanographic dataset derived from in situ measurements during 1919–2014. *Sci Data* 3:160029. <https://doi.org/10.1038/sdata.2016.29>
- Zhou W, Chan CL (2007) ENSO and the South China Sea summer monsoon onset. *Int J Climatol* 27:157–167
- Zhu Y, Sun J, Wang Y, Wei Z, Yang D, Qu T (2017) Effect of potential vorticity flux on the circulation in the South China Sea. *J Geophys Res*. <https://doi.org/10.1002/2016JC012375>
- Zu T, Xue H, Wang D, Geng B, Zeng L, Liu Q, Chen J, He Y (2019) Interannual variation of the South China Sea circulation during winter: intensified in the southern basin. *Clim Dyn* 52:1917–1933